UpWind

aerodynamics and aero-elasticity Rotor aerodynamics in atmospheric shear flow

Sørensen, Niels; Johansen, Jeppe

Published in:
Proceedings of The European Wind Energy Conference & Exhibition, EWEC 2007

Publication date:
2007

Document Version
Publisher's PDF, also known as Version of record

UPWIND, Aerodynamics and aero-elasticity
Rotor aerodynamics in atmospheric shear flow

Niels N. Sørensen
Wind Energy Department, Risø National Laboratory &
Department of Civil Engineering, Aalborg University

Jeppe Johansen
Wind Energy Department, Risø National Laboratory, Denmark

Summary:

Traditionally, rotor computations using CFD (Computational Fluid Dynamics) are performed assuming a uniform inflow with zero shear over the rotor disc. In the present work, time true simulations of a rotor in an atmospheric boundary layer are performed to investigate the unsteady effects due to variation of the mean velocity over the rotor disc. The main purpose of these computations are to provide new input to the BEM (Blade Element Momentum) type models used in most engineering codes, concerning the dynamic induction and an eventual phase shifting of the force response with respect to the variation of the inflow velocity over the rotor disc. The results show a clear disturbance of the flow upstream of the rotor and a pronounced phase lag in azimuth direction of the forces and the axial velocity seen by the blades.

Introduction

Most modern design codes for wind turbines utilize aerodynamics based on BEM methods, see [1, 2]. For modern large scale wind turbines with rotor diameters in the order of 100 meters, the influence of upstream turbine wakes, atmospheric turbulence and even the shear of the atmospheric velocity profile, will result in severe variation of the induction as function of the azimuth position of the blades. In the BEM method the implementation of these effects are not straight forward and more understanding of the actual flow physics is needed. In the present work the effect of severe wind shear, which has been observed during night time at the Test Station For Large Turbines at Høvsøre in Denmark will be investigated.

Typical rotor computations performed with CFD codes use the so-called Reynolds Averaged Navier-Stokes approach, where the effect of turbulence is modeled through an eddy viscosity assumption [3,4,5,6,7,8]. For all computations resolving the actual geometry of the rotor known by the authors, the simulations have utilized a uniform inflow velocity and assumed the incoming flow to be laminar. The reason why turbulent inflow is typically not simulated using RANS technique for rotor simulations can be seen by the following considerations. For a standard rotor computation, the turbulent boundary layer developing on the rotor blade surfaces is typically much thinner than 1 meter, even for the case where flow separation is present, which results in the eddy viscosity being approximately 1000 times the molecular viscosity. The viscosity of the turbulent atmospheric boundary layer, assuming a logarithmic velocity profile, results in the following well-known expression for the turbulent eddy viscosity as distance over terrain, $\nu_t = \kappa u_\tau z$. Thus simulating the atmospheric boundary layer using the RANS model, the eddy viscosity resulting from the earth boundary layer at hub height of a typical turbine would be of the order of $1x10^6$ compared to the molecular viscosity. Trying to simulate a rotor in the earth boundary layer would thus lead to an extremely low effective Reynolds number, making all attempts to represent the boundary layer on the rotor impossible.

High ratio of shear over the rotor disc is typically observed during nights with strongly stable boundary layers. For these situations the stable stratification of the atmosphere severely suppresses the mechanical turbulence, leaving the flow essentially laminar and with a very weak streamwise development. For a typically day time neutral boundary layer, with a surface roughness of ~0.01 [m] and a friction velocity of 0.6 [m/s] the mean axial velocity will vary around 2 [m/s] over a 100 diameter rotor. In the case of highly stratified flow, as observed during night time, the velocity may vary as much as 6 [m/s] over the rotor diameter. Focusing on stable boundary layers, the fact that the stream-wise development of the flow is low and the flow nearly laminar makes it possible to specify a shear profile at the inlet region of the computational domain, without any noticeable change in the flow direction see, Figure 2.

Method

The rotor computations are performed using the same spherical domain for the two scenarios, uniform inflow and severe vertical shear, with the domain centered on the rotor axis. In order to avoid negative velocities for $z \leq 0$ the power law used to specify the vertical shear profile is blended to a constant velocity profile near the location where the earth surface should have been located, see Figure 1.

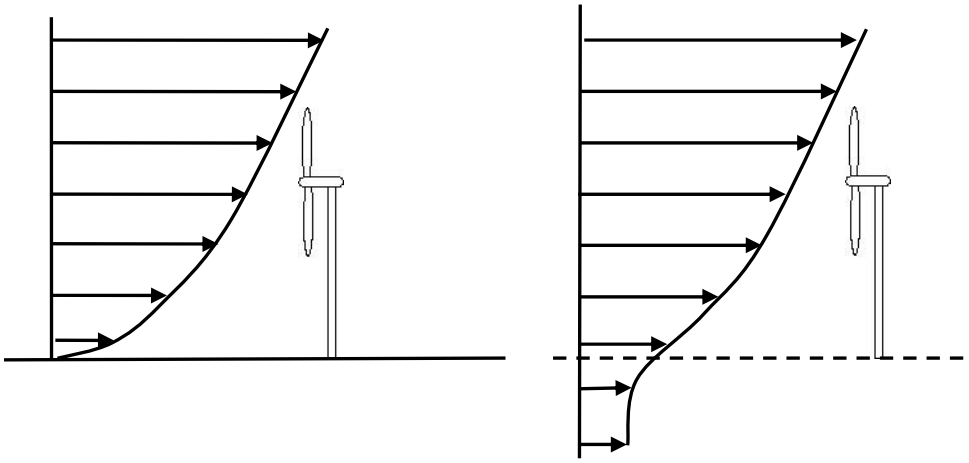

Figure 1 To avoid problems with negative velocity below ground level using a spherical domain, the shear profile is blended with a constant velocity profile below terrain level.

The shear profile of the velocity used in the present work is modeled in the following way

$$U(z) = U_{hub}\left[\beta(z/z_{hub})^{\alpha} + (1-\beta)\right] \text{ , where } \beta = \begin{cases} 1 & , z \succ z_{\lim} \\ \dfrac{\gamma}{\exp(1.0)}\exp\left(\dfrac{z+z_l}{z_{\lim}+z_l}\right) & , z \le z_{\lim} \end{cases},$$

where U_{hub} = 8 [m/s], α =0.55, z_{hub} = 90[m], z_l = 20 [m], z_{lim} = 25 [m] and γ = 0.75. To assure that the shear layer computations could be performed with the present approach, a single case using the mesh described later with the rotor at zero rotational speed was first computed. This should correspond to the case of a parked rotor, and we should expect very limited disturbance or induction from the rotor. Additionally, it should be possible to verify that the use of laminar conditions together with the high Reynolds number would results in minimal streamwise development of the enforced velocity shear profile. In Figure 2 a vertical velocity profile at the symmetry plane of the turbine is shown. In agreement with expectations minimal development is seen from far upstream to far downstream.

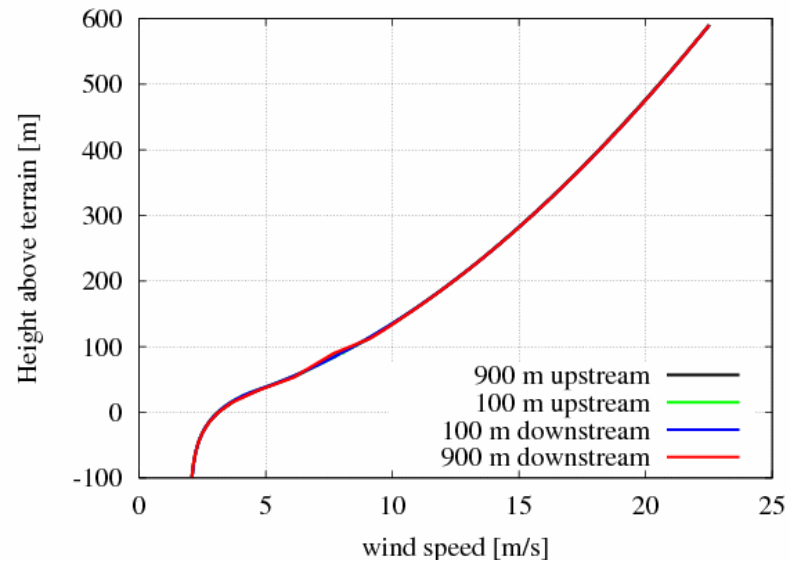

Figure 2 The development of the velocity profile from far upstream to far downstream for the case of the parked rotor.

Navier-Stokes Solver

The in-house flow solver EllipSys3D is used in all computations presented in the following. The code is developed in co-operation between the Department of Mechanical Engineering at the Technical University of Denmark and The Department of Wind Energy at Risø National Laboratory, see [9],[10], [11]. The EllipSys3D code is a multiblock finite volume discretization of the incompressible Reynolds Averaged Navier-Stokes (RANS) equations in general curvilinear coordinates. The code uses a collocated variable arrangement, and Rhie/Chow interpolation [12] is used

to avoid odd/even pressure decoupling. As the code solves the incompressible flow equations, no equation of state exists for the pressure, and in the present work the PISO algorithm of Issa [13] is used to enforce the pressure/velocity coupling. The EllipSys3D code is parallelized with MPI for executions on distributed memory machines, using a non-overlapping domain decomposition technique.
Both steady state and unsteady computations can be performed. For the unsteady computations the solution is advanced in time using a 2nd order iterative time-stepping (or dual time-stepping) method. In each global time-step the equations are solved in an iterative manner, using under relaxation. First, the momentum equations are used as a predictor to advance the solution in time. At this point in the computation the flowfield will not fulfil the continuity equation. The rewritten continuity equation (the so-called pressure correction equation) is used as a corrector making the predicted flowfield satisfy the continuity constraint. This two step procedure corresponds to a single sub-iteration, and the process is repeated until a convergent solution is obtained for the timestep. When a convergent solution is obtained, the variables are updated, and we continue with the next timestep.
For steady state computations, the global time-step is set to infinity and dual time stepping is not used, this corresponds to the use of local time stepping. In order to accelerate the overall algorithm, a multi-level grid sequence is used in the steady state computations. The convective terms are discretized using a third order QUICK upwind scheme, implemented using the deferred correction approach first suggested by Khosla and Rubin [14]. Central differences are used for the viscous terms, in each sub-iteration only the normal terms are treated fully implicit, while the terms from non-orthogonality and the variable viscosity terms are treated explicitly. Thus, when the sub-iteration process is finished all terms are evaluated at the new time level.
In the present work the turbulence in the boundary layer is modeled by the k-ω SST eddy viscosity model [15]. The equations for the turbulence model are solved after the momentum and pressure correction equations in every sub-iteration/pseudo time step.
The three momentum equations are solved decoupled using a red/black Gauss-Seidel point solver. The solution of the Poisson system arising from the pressure correction equation is accelerated using a multigrid method. In order to accelerate the overall algorithm, a multi-level grid sequence and local time stepping are used.
For the rotor computations with uniform inflow a steady state moving mesh approach is used [16], while for the shear layer computation a standard moving mesh formulation in a fixed frame of reference is used [17]. The moving mesh option has been implemented in the EllipSys3D solver in a generalized way allowing arbitrary deformation of the computational mesh, following [18]. It has been used for doing unsteady simulations for several years both for stiff rotors in yaw and fully coupled aeroelastic computations [17, 19, 20, 21]. For the present application of rotor in a shear flow, special care has to be taken with respect to the dependency of the inflow of the height over terrain, making the velocity at the inflow change when the mesh is rotated and thereby changing the physical location of the boundary points

Computational Grid
The rotor used in the present work, is designed in connection with the European UPWIND project, it is a three bladed rotor with a diameter of 126 meters, where the inner part of the blade uses DU airfoils and the outer part features the NACA64-XXX airfoils. The actual rotor design is heavily inspired by the design of the LM 61.5 rotor, see Figure 4.
Typically, computations of rotor power using CFD are performed for uniform inflow allowing the computations to exploit the periodicity in the azimuth direction. For turbines operating in the upwind configurations, the assumption that the effect of the tower and the nacelle are weak and can be neglected is typically used. In the present work only the rotor is modeled, but as we are investigating a case where non-uniform inflow are present, the full three bladed rotor is modeled. Based on experience with previous airfoil and rotor computations, 256 cells are distributed around the blade in chordwise direction, while 128 cells are used in the spanwise direction, and a square block of 64x64 cells are used at the blade tip to close the O-mesh 'tube', see Figure 3 left. In the normal direction 128 cells are used to march the grid to the farfield, starting with a cells size at the blade surface of ~$1x10^{-5}$ [m] assuring that the y+ is below two for the total blade surface. The total number of cells for the full three bladed rotor is around 14 million cells, and the outer boundary is placed ~10 rotor diameters away from the rotor centre.

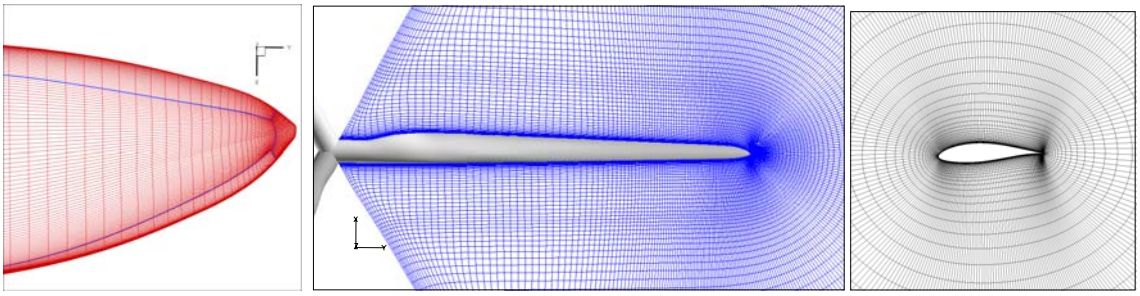

Figure 3 The square tip block (left picture), the spanwise resolution around the blade (centre picture), and the o-mesh around the chord (right picture).

At the blade surface no-slip wall boundary conditions are specified, while most of the outer boundary is specified as inflow conditions with the velocity prescribed in accordance with the undisturbed flow velocity, either uniform or given by the shear layer velocity profile. The remaining part of the outer boundary is specified as outlet conditions, where all flow quantities except the pressure is specified as fully developed, see Figure 4.

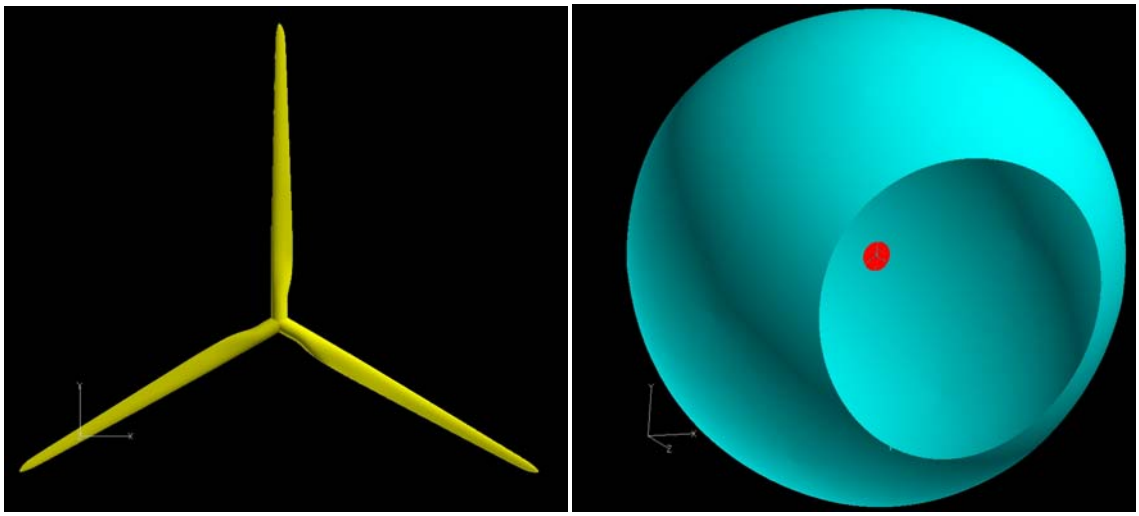

Figure 4 The three bladed UPWIND rotor, having a rotor diameter of 126 meter (left), and the full domain used for the rotor computations (right). The rotor disc is indicated in red to increase visibility; the inlet part of the outer spherical boundary is indicated in blue, while the remaining part of the spherical boundary is specified at outlet.

Results

The operational conditions used for the computations of the UPWIND rotor are listed in Table 1. In Figure 5 the computed mechanical power is shown, indicating a fair agreement with at standard BEM computations. The large deviation at high wind speed is mainly attributed to the estimated airfoil data used for the BEM computations. The figure additionally shows that the shear layer computation only predicts a small deviation of the averaged mechanical power production compared to the case with uniform inflow. This behavior can not be expected to be general, and may be attributed to the actual shape of the shear layer.

In Figure 6, the evolution of the low speed shaft torque is shown as function of rotor revolutions, exhibiting a very slow variation in time, indicating that even after fifty revolutions the rotor has still not reached a fully stable situation. In fact, due to the skewed nature of the wake, the situation may never stabilize. In Figure 5, the computed thrust force is shown for several wind speeds for the uniform inflow and for the single shear layer computation. Again, a very good agreement is observed between the averaged thrust for the two quite different conditions.

Table 1 The operational parameters for the UPWIND rotor, indicating the rotational speed and tip pitch used as function of wind speed.

Wind Speed $[m/s]$	Rotational Speed $[rad/s]$	Tip Pitch [deg]
8.0	0.964	0.0
11.0	1.267	0.0
15.0	1.267	10.36
20.0	1.267	17.42
25.0	1.267	23.11

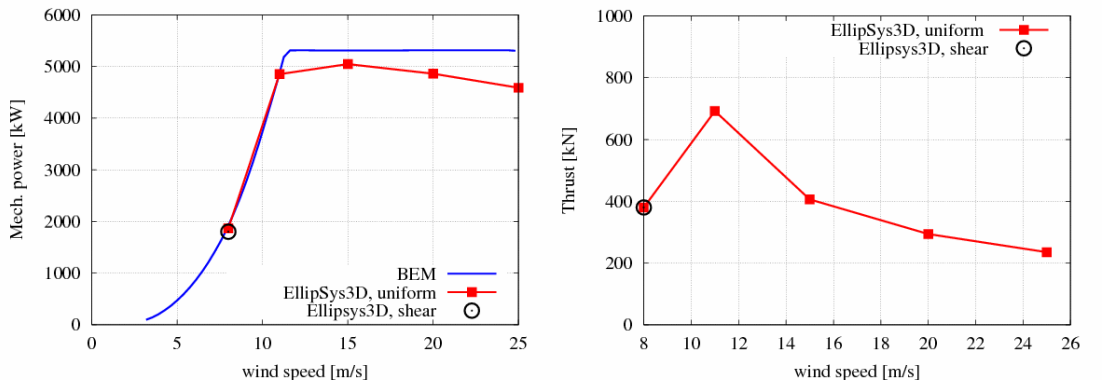

Figure 5 The left picture shows the computed mechanical power for the UPWIND rotor, computed using BEM and CFD for uniform inflow and the shear computations for 8 [m/s], while the right picture shows the computed thrust force using CFD for both uniform and the single non-uniform case at 8 [m/s].

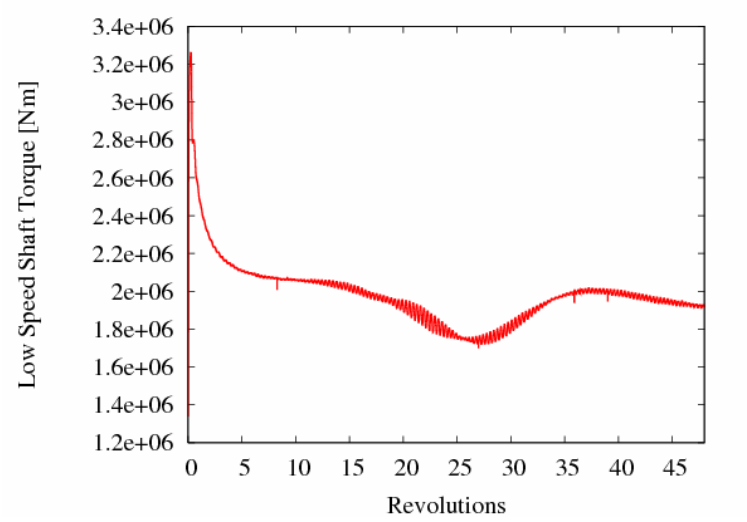

Figure 6 Time history of the low speed shaft torque for the shear computations, showing the very slow variation as function of revolutions.

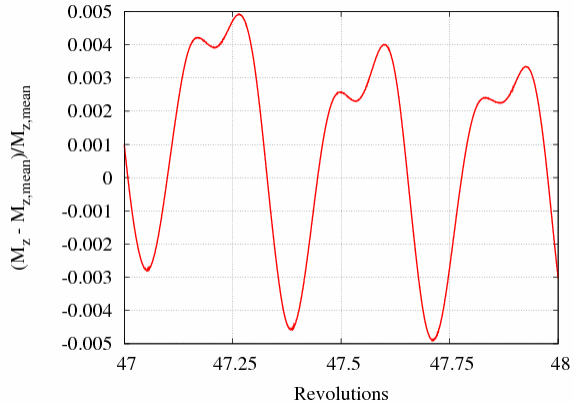

Figure 7 The variation of the low speed shaft torque as function of azimuth position, showing a clear 3D variation.

Another interesting observation about the mechanical power or low speed shaft torque can be seen from Figure 7 where the detailed variation of the shaft torque is shown for a single revolution. Neglecting the weak trend of the decreasing low speed shaft torque over time, a clear 3P variation of the torque can be observed. For a pure one-

dimensional linear shear in the vertical direction, the rotational sampling of the velocity by the blades combined with an assumption of the driving force being proportional to the instantaneous velocity and neglecting any influence of induction, the resulting shaft torque would be constant over a revolution. In the present case the shear is not linear, but a power law profile, and even without the assumption of no effect of induction this would lead to a variation of the shaft torque over a revolution.

Besides the inlet velocity profile deviating from the linear profile a strong influence of the induction is seen on the flow velocity experienced by the blades. In Figure 8 this is illustrated by the normalized axial force $(F_z-F_{z,mean})/F_{z,mean}$, and the normalized axial velocity $(U-U_{mean})/U_{mean}$ 2 and 50 meter upstream of the rotor at the same azimuth position, at three radial stations. Looking at the 20 meter radial station, see Figure 8, comparing the theoretical variation of the axial velocity with the ones experienced 2 and 50 meter upstream of the rotor, a clear effect of induction is observed as a large deviation can be seen. The actual velocities do not show the sinusoidal behavior of the theoretical velocity variation and additionally the curves are phase shifted so that the maximum and minimum are shifted aft of the theoretical curve. Comparing the velocity 2 meter directly upstream of the rotor with the velocity 50 meter upstream these are highly correlated and exhibit similar behavior. This behavior is also reflected in the axial force component and the tangential force component (not shown here), indicating a good correlation between the axial velocity and the actual force experienced by the blades. Looking at the 40 and 63 meter stations, it is clear that the phase shift diminishes with increasing radius and that both velocity and axial force variations become increasingly sinusoidal. From these figures it is clear that even though the shaft torque only varies very little, the blade forces vary as much as +/- 40 percent during a revolution, Figure 8.

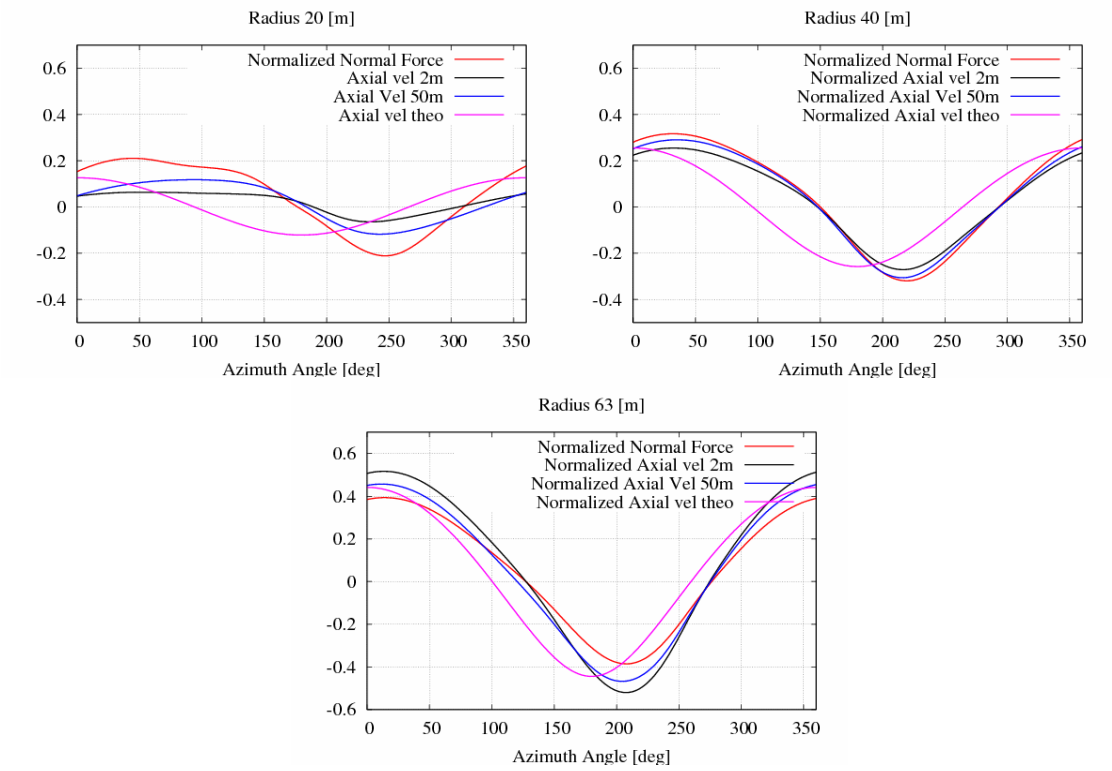

Figure 8 The azimuth variation of the normalized normal force and normalized axial velocity at the 20, 40 and 63 meters radial positions.

To obtain a more detailed picture of the variation of the blade forces, the spanwise force distribution is shown for four distinct azimuth positions, see Figure 9. When the blade is at the top position, at zero degrees azimuth, a relatively high load in both the axial and tangential direction is observed. Additionally, when the blade is at the bottom position, at 180 degrees azimuth position, both the tangential and the axial force is low as may be expected. The hysteresis effect can be seen at the 90 degrees and 270 degrees azimuth position, which with respect to the undisturbed shear profile experiences similar inflow conditions. Here the 90 degrees azimuth position is considerably higher loaded than the 270 degrees position. This is believed to be connected to the time history of the forces, where the 90 degrees case is following the high load case at zero degrees, while the 270 degrees case follows the low load case of 180 degrees.

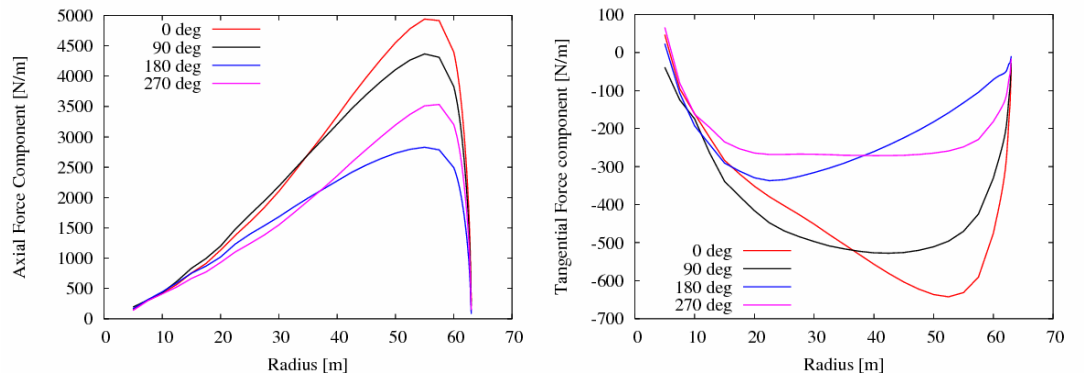

Figure 9 The azimuth variation of the tangential and axial force along the blade span for four azimuth angles, [0, 90, 180, 270] degrees.

Looking at the velocity profiles at a vertical slice through the symmetry plane of the turbine, the effect of the high induction can be observed in Figure 10, where the disturbance can be seen in the inflow velocities even 600 meters upstream of the rotor corresponding to approximately 5 rotor diameters. If this is representative for the actual behavior, it may severely influence the requirements for measuring the undisturbed flow in case of large velocity shear. The development of the velocity profile downstream corresponds qualitatively with wakes reported in the literature.

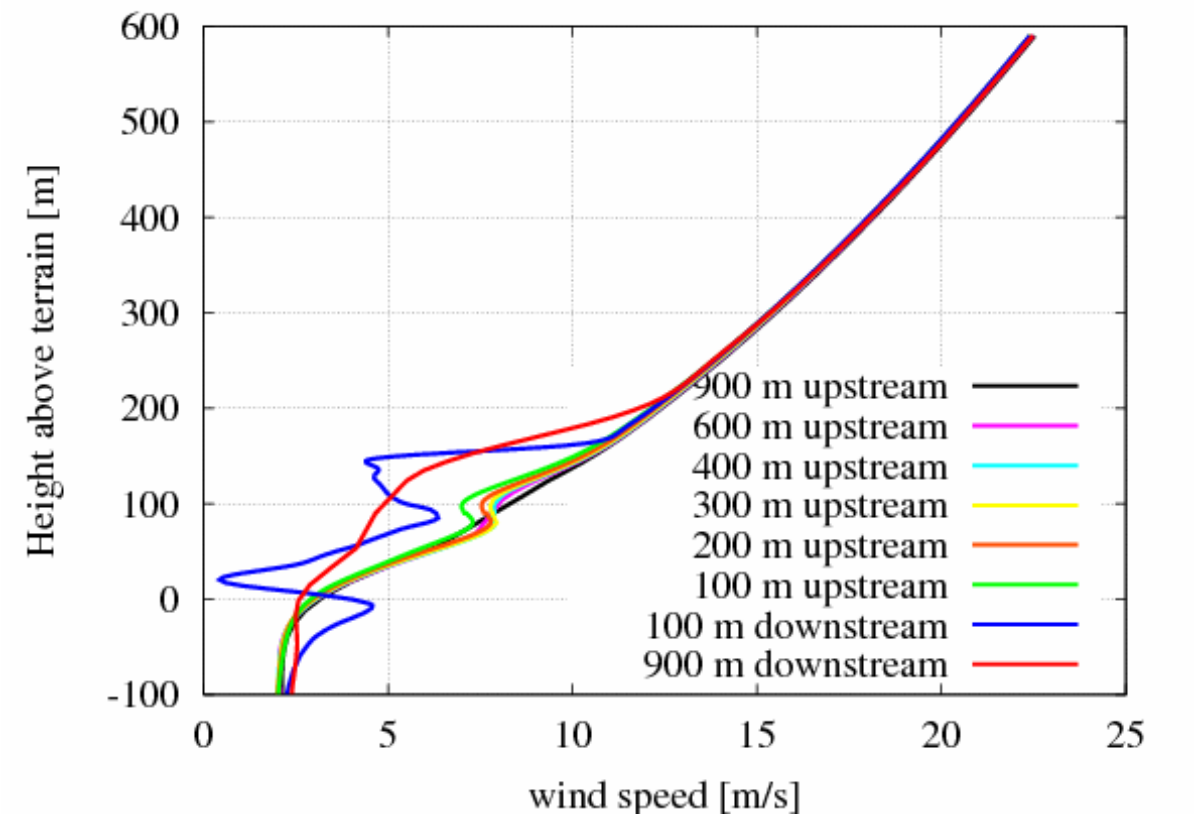

Figure 10 The velocity profile upstream and downstream of the UPWIND rotor.

Looking at the wake patterns, see Figure 11, the following aspects may be seen. The expected tilting of the rotor wake due to the velocity gradient is clearly visible, where the horizontal transport of the tip vortex is largest when in top position. Due to the variation of load with azimuth position, the rotor wake is no longer a perfect cylinder but is skewed with higher expansion at around the 135 degrees azimuth position.

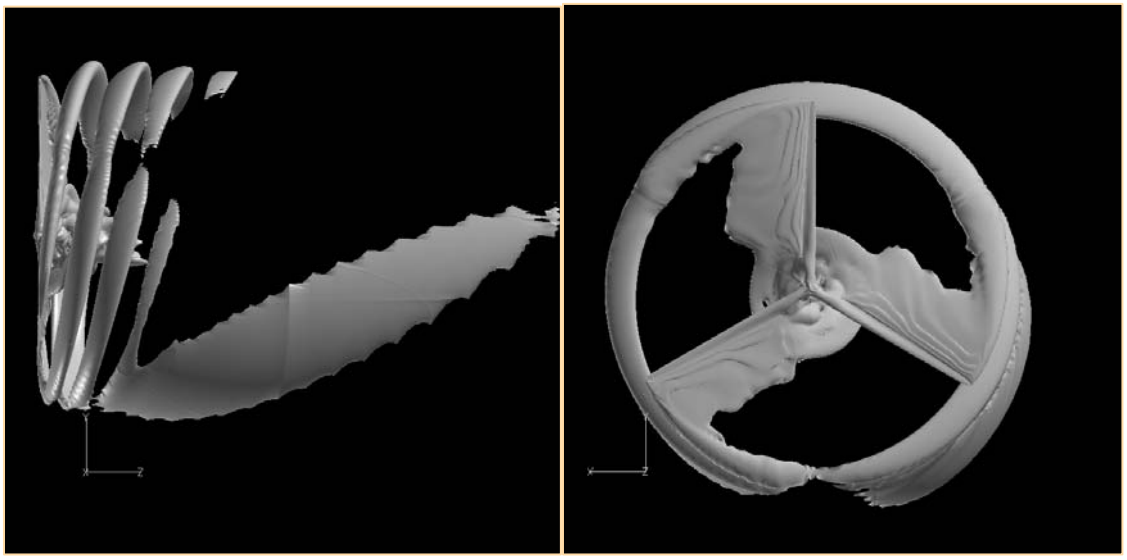

Figure 11 Iso-sheets of the absolute value of the vorticity showing the root, tip vortices and the trailing vortex sheet behind the rotor blades. The tilting of the wake due to the velocity gradient is evident especially in the right picture, while the left picture shows a very weak skewing of the wake due to the azimuth variation of the loading of the rotor.

Conclusion

A rotor computation in severe shear has been computed and compared to the situation in uniform inflow. Both the thrust and mechanical power for the shear computations show good agreement with the computations for uniform flow. Looking at the variation of the mechanical power over a revolution, a clear 3P variation is found even though the amplitude of the variation is below one percent. The corresponding variation of the individual blade forces show much greater variation, with a maximum variation of nearly 40 percent compared to the mean value. Inspection of the azimuth variation of the blade forces and the inflow velocity close to the blades indicates a variation which deviates severely from the theoretical sinusoidal variation, especially at the inboard stations. The phase shift of this behavior compared to the theoretical curve is largest at the inboard stations, while the phase shift diminishes toward the blade tip.

This hysteresis effect of the individual blade loads as well as the upstream velocities as function of the azimuth position is clearly reflected in the wake velocities.

Acknowledgement

The work was funded by the European Union under contract SES6 No 019945 UPWIND and the Danish Energy Agency under contract ENS-33031-0083, Computations were made possible by the use of the MARY PC-cluster at Risø National Laboratory and the DCSC, PC-cluster Yggdrasil.

References

[1] Hansen A.C. and Butterfield C.P. Aerodynamics of Horizontal-Axis Wind Turbines, Annu. Rev. Fluid Mech. 1993. 25: 115-49

[2] Snel H., Review of the Present Status of Rotor Aerodynamic. Wind Energ., 1, 46-69. 1998

[3] Sørensen N.N., Michlesen J.A. and Schreck S. Navier-Stokes predictions of the NREL Phase VI rotor in the NASA Ames 80-by-120 wind tunnel. AIAA-2002-0032. 2002.

[4] Xu G. and Sankar L.N. Application of a Viscous Flow Methodology to the NREL Phase VI ROTOR. AIAA-2002-0030. 2002.

[5] Benjanirat S., Sankar L.N. Recent Improvements to a Combined Navier-Stokes Full Potential Methodology for Modeling Horizontal Axis Wind Turbines., AIAA-2004-0830, 2004.

[6] Duque E.P.N., Burklund M.D. and Johnson W., Navier-Stokes and Comprehensive Analysis Performance Predictions of the NREL Phase VI Experiment, AIAA-2003-0355, 2003.

[7] Benjanirat S., Sankar L.N., Evaluation of Turbulence Models for the Prediction of Wind Turbine Aerodynamics, , AIAA-2003-0517. 2003.

[8] Tongchitpakdee C., Benjanirat S., Sankar L.N., Numerical Simulation of the Aerodynamics of Horizontal Axis Wind Turbines Under Yawed Flow Conditions, AIAA-2005-0773.

[9] Michelsen, J.A.. Basis3D - a Platform for Development of Multiblock PDE Solvers. Technical Report AFM 92-05, Technical University of Denmark, 1992.

[10] Michelsen J.A., ”Block structured Multigrid solution of 2D and 3D elliptic PDE's”, Technical Report AFM 94-06, Technical University of Denmark, 1994.

[11] Sørensen, N.N.. General Purpose Flow Solver Applied to Flow over Hills. Risø-R- 827-(EN), Risø National Laboratory, Roskilde, Denmark, June 1995.

[12] Rhie C.M. ”A numerical study of the flow past an isolated airfoil with separation” Ph.D. thesis, Univ. of Illinois, Urbane-Champaign, 1981.

[13] Issa R.I. Solution of the implicitly discretised fluid flow equations by operator-splitting’ J. Comp. Pys., 61, 1985

[14] Khosla P.K. and Rubin S.G., ”A diagonally dominant second-order accurate implicit scheme”, Computers Fluids, 2:207-209, 1974.

[15] Menter F.R., ”Zonal Two Equation k-ω Turbulence Models for Aerodyanmic Flows”. AIAA-paper-932906, 1993.

[16] Sørensen, N.N., Rotor computations using a 'Steady State' moving mesh. IEA Joint Action Committee on aerodynamics, Annex XI and 20. Aero experts meeting, Pamplona (ES), 25-26 May 2005.

[17] Sørensen, N.N.; Michelsen, J.A., and Schreck S.,Application of CFD to Wind Turbine Aerodynamics. In: CD-Rom proceedings. 4. GRACM congress on computational mechanics, Patras (GR), 27-29 Jun 2002. Tsahalis, D.T. (ed.), (Greek Association of Computational Mechanics, [s.l.], 2002) 9 p.

[18] Demirdzic, I., Peric, M. (1988): Space conservation law in finite volume calculations of fluid flow. Int. J. Numer. Methods Fluids, 8, 1037-1050.

[19] Madsen, H.A.; Sørensen, N.N.;Schreck, S.,YAW AERODYNAMICS ANALYZED WITH THREE CODES IN COMPARISON WITH EXPERIMENT, 22rd ASME Wind Energy Symposium, RENO NV(US), 6-9 Jan 2003.

[20] Bertagnolio, F.; Gaunaa, M.; Hansen, M.; Sørensen, N.N.; Rasmussen, F., Computation of aerodynamic damping for wind turbine applications. In: CD-Rom proceedings. 4. GRACM congress on computational mechanics, Patras (GR), 27-29 Jun 2002. Tsahalis, D.T. (ed.), (Greek Association of Computational Mechanics, [s.l.], 2002) 8 p.

[21] Bertagnolio, F.; Gaunaa, M.; Sørensen, N.N.; Hansen, M.; Rasmussen, F., Computation of Modal Aerodynamic Damping Using CFD, 22rd ASME Wind Energy Symposium, RENO NV(US), 6-9 Jan 2003.